Mechanism of Stabilization of Helix Secondary Structure by Constrained Cα-Tetrasubstituted α-Amino Acids

Irene Maffucci,[a] *Sara Pellegrino,*[a] *Jonathan Clayden*[b] *and Alessandro Contini*[a]*

[a] Dipartimento di Scienze Farmaceutiche – Sezione di Chimica Generale e Organica "Alessandro Marchesini", Università degli Studi di Milano, Via Venezian, 21 20133 Milano, Italy.

[b] School of Chemistry, University of Manchester, Oxford Road, Manchester, M13 9PL, UK.

KEYWORDS

peptide folding; non-canonical amino acids; replica exchange molecular dynamics; potential of mean force; weak hydrogen bonds; AIM analysis.

ABSTRACT

The theoretical basis behind the ability of constrained Cα-tetrasubstituted amino acids (CTAAs) to induce stable helical conformations has been studied through Replica Exchange Molecular Dynamics, Potential of Mean Force and Quantum Theory of Atoms In Molecules calculations on Ac-L-Ala-CTAA-L-Ala-Aib-L-Ala-NHMe peptide models. We found that the origin of helix stabilization by CTAAs can be ascribed to at least two complementary mechanisms limiting the

backbone conformational freedom: steric hindrance predominantly in the (+x,+y,-z) sector of a right-handed 3D Cartesian space, where the z axis coincides with the helical axis and the Cα of the CTAA lies on the +y axis (0,+y,0), and the establishment of additional and relatively strong C-H···O interactions involving the CTAA.

Introduction

Many biological events are caused by protein-protein interactions (PPIs),[1] often involving helical motifs.[2] Much attention has been paid to the development of synthetic bioactive peptides targeting PPIs.[3-4] A well-designed peptide can indeed show greater selectivity and specificity, and lower toxicity, than classical drug-like molecules.[5-7] However, the use of peptides can be affected by drawbacks such as low bioavailability, metabolic degradation and poor conformational stability.[8] To overcome these limitations, non-proteinogenic amino acids (AA) may be inserted in the sequence to provide peptides that are inherently stable to proteases and peptidases,[9] and that fold into well-ordered secondary structures.[10-11]

A widely exploited class of non-proteinogenic AAs is that of the Cα-tetrasubstituted AAs (CTAAs), which act as helix-stabilizers by limiting the conformational freedom of the peptide backbone.[5, 12-20] Among these, the most studied are α-aminoisobutyric acid (Aib), which stabilizes α- or 3_{10}-helices depending on the peptide chain length,[21-23] its higher homologues such as Cα,α-diethylglycine, found to stabilize an extended conformation known as the 2.0_5 helix,[15, 24] and cyclic derivatives such as 1-aminocyclopropane-1-carboxylic acid (Ac_3c) and 1-aminocyclopentane-1-carboxylic acid (Ac_5c), which stabilize helices and other turn-like conformations.[25-27] Moreover, with chiral CTAAs, the stability of helical secondary structures depends on the configuration at Cα of the CTAA relative to the screw-sense of the helix. Thus,

chiral CTAAs may induce a preferred screw-sense preference in an otherwise achiral peptide chain.[10, 28-42]

Although different CTAAs have been exploited in the preparation of stable foldamers,[10, 30, 43] and new CTAAs are constantly being developed,[44-48] intuitive descriptors that could be used to predict how a given CTAA can drive peptide folding, or to compare different CTAAs in terms of stabilization efficacy, are, to our knowledge, not yet defined.

In this article we discuss the theoretical investigation of a selection of chiral constrained CTAAs (Figure 1), some of them experimentally shown to be helix-stabilizers,[10] which aims to explain, at an atomistic level, the reason for their conformational behavior.

This objective was pursued by using Replica Exchange Molecular Dynamics (REMD),[49] which reproduces the experimental folding behavior of several peptides of small to medium length,[50-52] and Quantum Theory of Atom in Molecules (QTAIM) which, by locating bond critical points (BCP) and corresponding bond paths (BP),[53] allows a quantitative characterization of non-bonded interactions, found to be critical in the stabilization of secondary structures.[54-58]

We find that the insertion of CTAAs in Ac-L-Ala-CTAA-L-Ala-Aib-L-Ala-NHMe model peptides, a system used in similar studies previously reported,[10, 59] limits the backbone conformational freedom through at least two complementary mechanisms: 1) steric hindrance predominantly in the (+x,+y,-z) sector of a right-handed 3D Cartesian space (Figure 2), where the +z→-z axis coincides with the N→C helical axis and the Cα of the CTAA lies on the +y axis (0,+y,0) and 2) the generation of additional intramolecular C-H···O interactions.

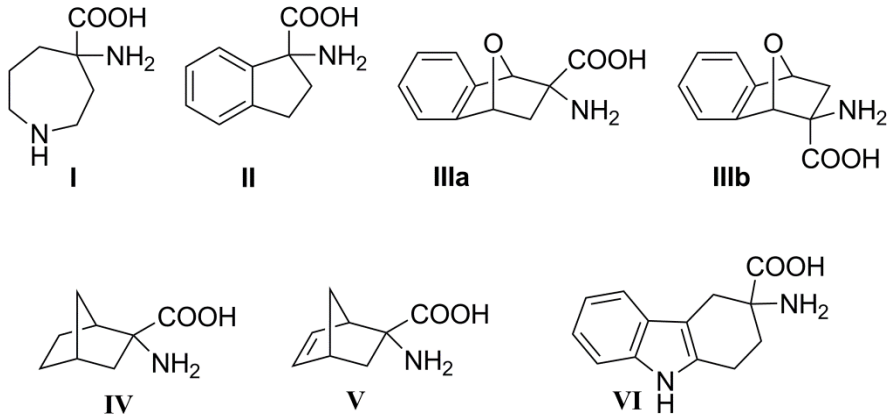

Figure 1. A selection of CTAAs reported by literature.[10, 47-48, 60-62]

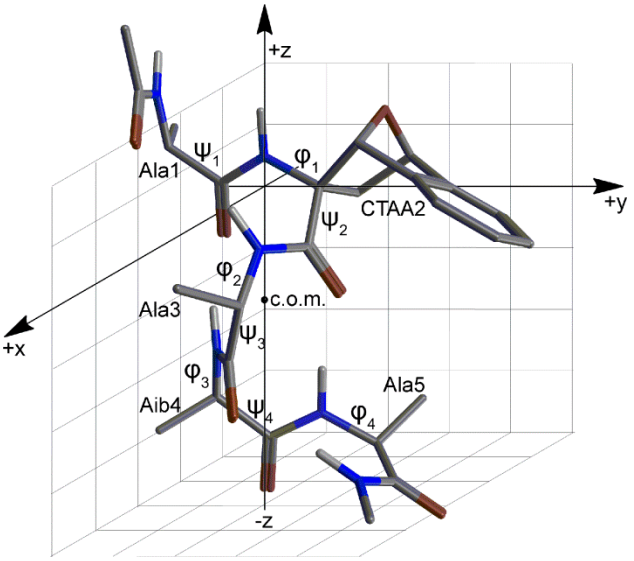

Figure 2. 3D Cartesian space used to represent peptides containing CTAAs. The most representative geometry from cluster analysis of Ac-L-Ala-(1*R*,2*S*,4*R*)-**IIIb**-L-Ala-Aib-L-Ala-NHMe is shown; c.o.m. = center of mass.

Methods

REMD simulations. CTAAs were designed using MOE,[63] capped respectively with an acetyl (Ac) and a NHMe group at the N- and C-termini and submitted to a "Low Mode" conformational search (MMFF94x force field, Born solvation, iteration limit = 40000, MM iteration limit = 2500, rejection limit = 500). The two lowest energy conformations having φ and ψ dihedrals

matching a right- or a left-handed helix (φ = ±60°, ψ = ±45°) were selected to derive partial charges with the R.E.D.IV software.[64] Each geometry was optimized at the HF/6-31G(d) level and two different spatial orientations were used to derive orientation- and conformation-independent RESP-A1 charges. Charge restraints of −0.4157, 0.2719, 0.5973 and −0.5679 were imposed to the backbone nitrogen, hydrogen, carbonyl carbon and oxygen, respectively, as observed for standard AAs in the AMBER *ff99SB* force field.[65]

REMD simulations were carried out on each Ac-L-Ala-CTAA-L-Ala-Aib-L-Ala-NHMe peptide by starting from an extended conformation (ψ=φ=ω= 180°). The simulation protocol was previously optimized to reproduce the X-ray conformation of Boc-L-Ala-Aib-L-Ala-Aib-Aib-OMe[66] and further validated through the reproduction of both NMR and X-ray geometries of related CTAA containing pentapeptides.[10, 59] It is known that several polypeptide force fields are affected by a certain degree of helical propensity.[67-70] Thus, we preliminarily evaluated the ability of different force field and solvent model combinations to reproduce the folding of a selection of helical, turn-like and random coil peptides, made by 5-15 residues, and ff99SB coupled with the implicit solvent model by Onufriev, Bashford, and Case (igb = 5).[71] provided the best agreement with the available experimental data (results are available from the authors upon request). Our impression is that, with this method, the overall helical content is slightly overestimated, but this error, being systematic, should not affect the comparison of different CTAAs. Briefly, 12 replicas were run at temperatures from 260.00 to 658.94 K, using the *ff99SB*/igb = 5 force field and solvent model combination. The protocol details, given elsewhere,[10] were modified in the present study only in the simulation length, which was raised up to 250 ns per replica, for a total of 3 μs of simulation for each peptide. REMD simulations were conducted with the *pmemd* module of the Amber12 suite.[72] The trajectories were extracted

at 308.53 K, unless stated otherwise. The simulation convergence was assessed on the basis of cluster analyses performed at 50-100, 100-150, 150-200 and 200-250 ns time intervals. We considered a simulation converged when the standard deviation of the main cluster population ($\sigma_{pop\%}$), averaged with respect to the different intervals, was below 5%. Cluster analyses were performed with *ptraj* by using the average-linkage algorithm and by sampling one every four frames.[72] The pairwise mass-weighted root mean squared displacement (RMSD) on Cα was used as a metric and a total of five clusters were requested on the basis of pseudo-F statistics and SSR/SST ratio.[73] Secondary structure analyses were performed by DSSP[74] on the 50-250 ns trajectories every Δt = 50 ns, coherently with cluster analyses, using the *ptraj* "secstruct" command. H-bonds were analyzed with VMD 1.9.1[75] over the whole 250 ns trajectory, with a donor−acceptor distance threshold of 4.0 Å and an angle cutoff of 30°. Only H-bonds with an occupancy ($occ_{\%}$) greater than 5% were considered.

2D and 3D Potentials of Mean Force (PMF) were obtained with Amber software coupled with the Weighted Histogram Analysis Method (WHAM) and WHAM-2d,[76] respectively. PMF were calculated over the 250 ns trajectory by setting a histogram limit of ±180°, 100 bins and a tolerance of 0.01. Selected dihedrals (φ_1, φ_2, ψ_2 and ψ_3, accordingly to Figure 2) were obtained from the REMD trajectories at 260, 283, 308 and 335 K.

QTAIM calculations. Selected geometries were fully optimized with Gaussian09[77] at the MPWB95/6-31+G(d,p) level,[78] a method that had proved reliable in previous studies from our group,[79] with the CPCM solvation model for water.[80] Vibrational analyses were performed at the same level to confirm optimized geometries as a minimum (no imaginary frequencies observed). QTAIM calculations were performed with AIM2000 on the obtained wave functions.[81] The maximum number of Newton iterations and the step-size were set to 400 and 0.5, respectively,

while other parameters were left as default. N-H···O, C-H···O and backbone N···O BCPs were analyzed and the electronic density ($\rho(r_c)$), the sign of the Laplacian ($\nabla^2(r_c)$), and the ellipticity (ε) were used to characterize the BCP network in terms of strength, type and stability of each BCP. BCPs with $\varepsilon > 1$ were considered as unstable and consequently discarded.

Results and Discussion

Conformational analysis. Table 1 reports results from cluster and DSSP analyses, while Table 2 shows results of the H-bond analysis of the REMD trajectories of peptides **1-15**.

Table 1. Average Helical Population from Cluster Analysis ($pop_{h\%}$) and Average DSSP Helical Content ($h_{\%}$)[a] Obtained from the REMD Trajectories of Ac-L-Ala-CTAA-L-Ala-Aib-L-Ala-NHMe Peptides **1-15**.[b] Differences Between Peptides Containing CTAAs of Opposite Stereochemistry ($\Delta pop_{h\%}$ and $\Delta h_{\%}$) are also Reported.

#	(*R*)-CTAAs[c]	$pop_{h\%}$	$h_{\%}$	#	(*S*)-CTAA[c]	pop_h%	h%	$\Delta pop_{h\%}$	$\Delta h_{\%}$
1	(*R*)-**I**[10]	43.2±3.3	46.7±1.0	**8**	(*S*)-**I**	n.a.[d]	23.1±1.2	0.5	23.5
2	(*R*)-**II**[47]	85.1±0.9	85.8±0.6	**9**	(*S*)-**II**	76.6±3.1	68.1±1.7	8.5	17.7
3	(1*R*,2*R*,4*R*)-**IIIa**[e]	73.3±2.0	80.0±0.2	**10**	(1*S*,2*S*,4*S*)-**IIIa**[e]	72.2±1.7	73.6±1.8	1.1	6.4
4	(1*S*,2*R*,4*S*)-**IIIb**[e]	79.7±1.5	82.0±0.7	**11**	(1*R*,2*S*,4*R*)-**IIIb**[e]	90.4±1.8	90.5±0.4	-20.3	-8.5
5	(1*S*,2*R*,4*R*)-**IV**	61.9±2.6	56.5±1.4	**12**	(1*R*,2*S*,4*S*)-**IV**[f]	30.6±2.7[e]	35.8±1.1	31.3	20.7
6	(1*R*,2*R*,4*R*)-**V**	82.5±1.6	82.9±0.5	**13**	(1*S*,2*S*,4*S*)-**V**	84.8±2.1	69.0±0.8	-2.3	+13.9
7	(*R*)-**VI**	83.1±2.4	84.1±1.3	**14**	(*S*)-**VI**	81.6±1.8	73.5±1.1	1.5	10.6

[a] Calculated as the sum of 3_{10}- and α-helix content of CTAA, averaged with respect to the 50-100, 100-150, 150-200 and 200-250 ns time intervals. [b] The $pop_{h\%}$ and $h_{\%}$ values obtained from the REMD trajectory of the reference Ac-Ala-Aib-Ala-Aib-AlaNHMe peptide **15** are 51.3±4.9 and 51.8±1.2, respectively. [c] The stereochemical descriptor refers to the Cα configuration. [d] The representative geometry of the most populated cluster does not correspond to a helix. [e] Experimental **IIIa**:**IIIb** ratio = 7:1.[12, 48] [f] The representative geometry of the most populated cluster corresponds to a left-handed helix.

Table 2. H-bond Analysis of REMD Trajectories of Ac-L-Ala-CTAA-L-Ala-Aib-L-Ala-NHMe Peptides **1-15** (donor: N-H; acceptor: C=O).[a]

#	CTAA	donor	acceptor	occ%	#	CTAA	donor	acceptor	occ%
1	(*R*)-**I**	Aib4	Ala1	39.00	**8**	(*S*)-**I**	Aib4	Ala	Aib4
		Ala5	**I**	12.94			Ala5	**I**	Ala5
		Ala5	Ala1	7.11					n.d.[b]
2	(*R*)-**II**	Aib4	Ala1	69.72	**9**	(*S*)-**II**	Aib4	Ala1	62.91
		Ala5	**II**	57.57			Ala5	**II**	52.06
3	(1*R*,2*R*,4*R*)-**IIIa**	Aib4	Ala1	64.15	**10**	(1*S*,2*S*,4*S*)-**IIIa**	Aib4	Ala1	60.07
		Ala5	**IIIa**	47.11			Ala5	**IIIa**	51.79
4	(1*S*,2*R*,4*S*)-**IIIb**	Aib4	Ala1	63.84	**11**	(1*R*,2*S*,4*R*)-**IIIb**	Aib4	Ala1	72.81
		Ala5	**IIIb**	58.91			Ala5	**IIIb**	65.69
5	(1*S*,2*R*,4*R*)-**IV**	Aib4	Ala1	41.55	**12**	(1*R*,2*S*,4*S*)-**IV**	Aib4	Ala1	31.89
		Ala5	**IV**	25.30			Ala5	**IV**	38.40
		Ala5	Ala1	11.20					n.d.[b]
6	(1*R*,2*R*,4*R*)-**V**	Aib4	Ala1	65.78	**13**	(1*S*,2*S*,4*S*)-**V**	Aib4	Ala1	62.08
		Ala5	**V**	55.69			Ala5	**V**	60.69
7	(*R*)-**VI**	Aib4	Ala1	70.17	**14**	(*S*)-**VI**	Aib4	Ala1	72.60
		Ala5	**VI**	60.13			Ala5	**VI**	54.16

[a]The reference H-bonds occ% obtained from the REMD trajectory of the Ac-Ala-Aib-Ala-Aib-AlaNHMe peptide **15** are 4→1 45.01%, 5→2 26.55% and 5→1 6.82%.[b] Not detected.

The average population of helical geometries ($pop_{h\%}$) and the DSSP helical content ($h_{\%}$), as well as φ and ψ dihedrals of the most representative structures obtained from cluster analysis (Table S1, S.I.), show that the considered peptides fold into a right-handed 3_{10}-helix, except for **8** and **12**. The former peptide, containing (*S*)-**I** (Figure 1), was previously shown by circular dichroism (CD), recorded in MeOH, and NMR experiments, performed in CD_3CN solution, not to fold into well-ordered secondary structures.[10] The latter peptide contains (1*R*,2*S*,4*S*)-**IV** and,

interestingly, is the only one showing a left-handed helix as the most populated cluster ($pop_{h\%}$ = 30.6±2.7). However, a minor amount of left-handed helix can also be observed for peptides **15**, **1** and **5** (CTAA = Aib, (*R*)-**I** and (1*S*,2*R*,4*R*)-**IV**, respectively).

Accordingly to cluster and DSSP analyses, the highest helical structuration is observed for peptides **11** (CTAA = (1*R*,2*S*,4*R*)-**IIIb**), **2** (CTAA = (*R*)-**II**), **7** (CTAA = (*R*)-**VI**) and **6** (CTAA = (1*R,2R,4R*)-**V**), all having $pop_{h\%}$ and $h_{\%}$ values above 80%. It can be noted that, among these CTAAs, (1*R*,2*S*,4*R*)-**IIIb** is the only one with an *S* configuration at Cα. Indeed, similarly to what theoretically predicted and experimentally observed for **I**,[10] the stereochemistry at Cα seems to influence, although to different extents, the ability of each CTAA to stabilize helical secondary structures and in all examples a "eutomer" (the enantiomer with the highest stabilization effect) and a "distomer" (the enantiomer with the lowest stabilization effect) can be observed, a classification which, however, depends on the stereochemistry of the other AA present in the chain.

A significant effect of Cα stereochemistry on both $pop_{h\%}$ and $h_{\%}$ was found for **IV** ($\Delta pop_{\%}$ = 31.3; $\Delta h_{\%}$ = 20.7), characterized by the norbornane core, with the (1*S*,2*R*,4*R*) enantiomer being the eutomer. An *R* configuration at Cα of CTAAs also leads to a higher helical propensity in peptides containing **I**, **II**, **V**, **VI** and **IIIa**, this last being the CTAA with the lowest difference among opposite stereochemical configurations ($\Delta pop_{\%}$ = 1.1; $\Delta h_{\%}$ = 6.4). H-bond analyses (Table 2), in accordance with cluster and DSSP analyses, generally showed stable $i+3 \rightarrow i$ H-bonds typical of the 3_{10}-helix, with occupancies of 50-70% of the total simulation time. Only the trajectories of peptides **1**, **5** and 1**5**, based on (*R*)-**I**, (1*S*,2*R*,4*R*)-**IV** and Aib, respectively, showed the presence of a $i+4 \rightarrow i$ H-bond, typical of α-helices, although with limited occupancies (7.11%, 11.2% and 6.82%, respectively). Surprisingly, the behavior of the norbornane

(1*S*,2*R*,4*R*)-**IV** is significantly different from that of the highly related norbornene (1*R*,2*R*,4*R*)-**V** and a possible reason will be given later.

These observations are supported by 3D-PMF analyses, which provide a clear indication on the statistical accessibility of selected dihedral pairs in the REMD trajectory. 3D-PMF were computed for φ_1-ψ_2 and φ_2-ψ_3 dihedral pairs (Figure 3 and S1, S.I.), belonging to the CTAA and CTAA+1 residues.

In the PMF profiles we generally observed a global minimum corresponding to a right-handed helix, and a local minimum corresponding to a left-handed helix. Among the CTAAs considered, (1*R*,2*R*,4*R*)-**V** and (1*R*,2*S*,4*R*)-**IIIb** appear to be the most selective toward a right-handed helix. Indeed, for peptides **1**, **3**, **5** and **15**, PMF(φ_1-ψ_2) profiles showed the presence of additional local minima, corresponding to β-strands or polyproline helices (Figure 3). These geometries appear to be statistically more accessible for peptide **15**, having Aib at position 2, followed by **5** ((1*S*,2*R*,4*R*)-**IV**), **3** ((1*R*,2*R*,4*R*)-**IIIa**) and **1** ((*R*)-**I**). Peptide **2**, containing the indane CTAA (*R*)-**II**, shows an additional minimum in a region that does not correspond to a well-defined secondary structure ($-130 \leq \varphi_1 \leq -180$ deg.; $-60 \leq \psi_2 \leq +30$ deg.) while peptide **7**, containing the tetrahydrocarbazole CTAA (*R*)-**VI**, shows only the minima corresponding to right- and left-handed helices, but with a ΔE between the two that is apparently lower than that observed for peptides **6** and **11**. Similar findings were shown by 3D-PMF(φ2-ψ3) profiles (Figure S1, S.I.), although the minimum corresponding to the right-handed helix has, for all the peptides, a larger basin than that observed for the φ_1-ψ_2 dihedral pair.

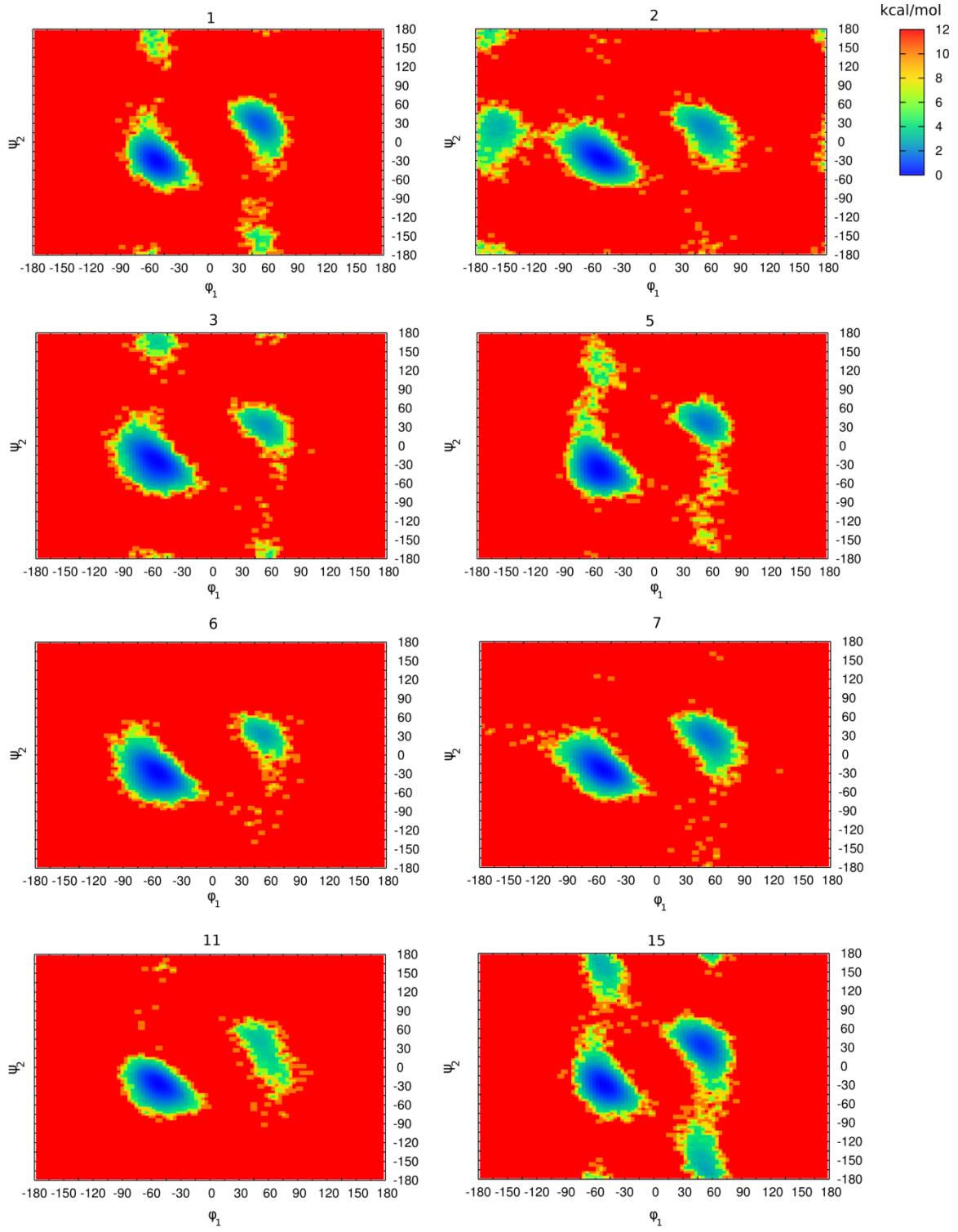

Figure 3. PMF profiles (kcal/mol) as a function of φ_1-ψ_2 dihedral pairs obtained from the REMD simulation of peptides **1-3**, **5-7**, **11** and **15** containing the eutomer CTAAs (*R*)-**I**, (*R*)-**II**, (1*R*,2*R*,4*R*)-**IIIa**, (1*S*,2*R*,4*R*)-**IV**, (1*R*,2*R*,4*R*)-**V**, (*R*)-**VI**, (1*R*,2*S*,4*R*)-**IIIb** and Aib, respectively.

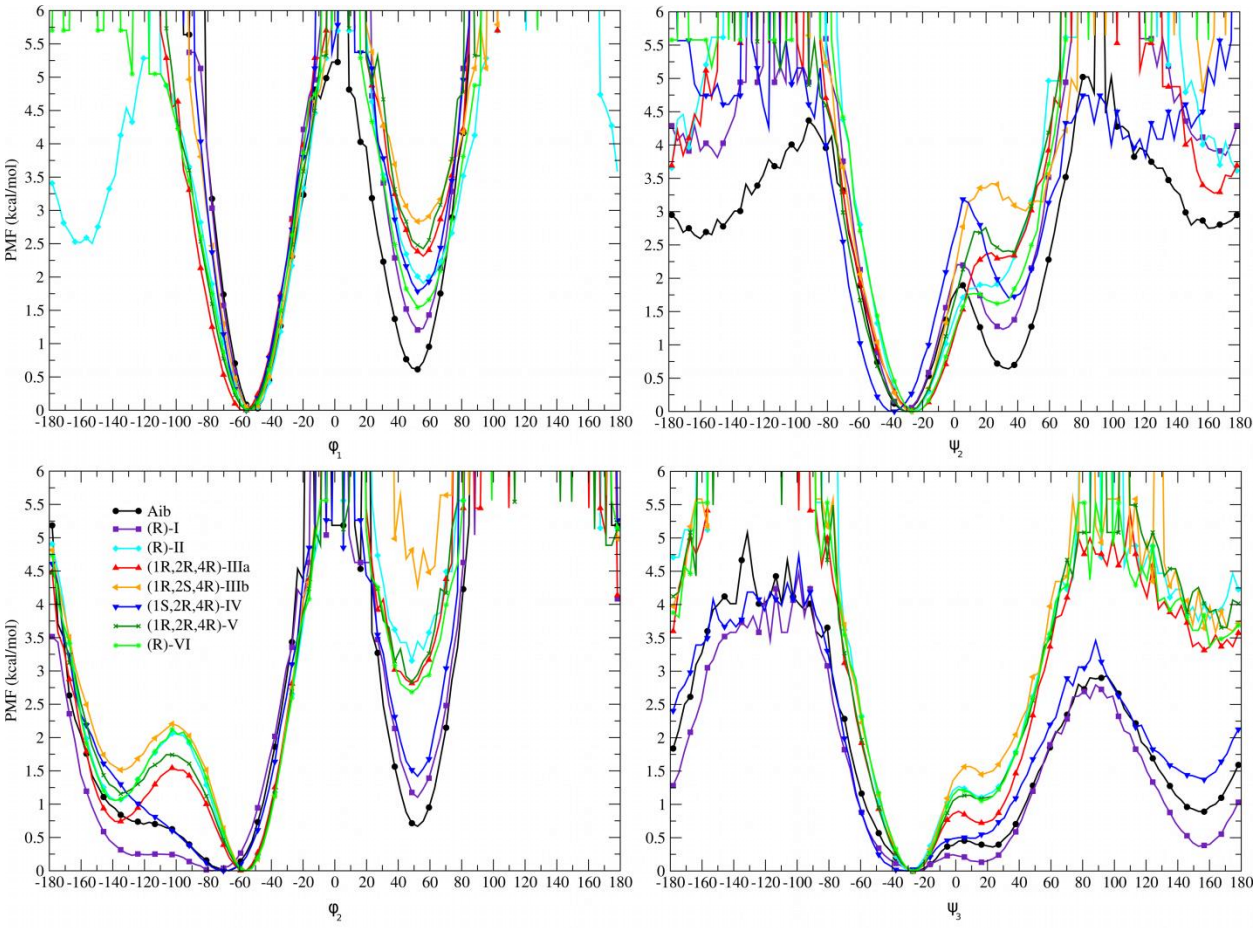

Figure 4. 2D-PMF profiles from the analyses of 260, 283, 308 and 335 K trajectories of peptides containing Aib and the CTAA eutomers. Dihedrals associated with PMFs higher than 6 kcal/mol were not sampled at the selected temperatures.

2D-PMF were also evaluated to obtain a more detailed description of the ΔE associated with the rotation of individual dihedrals (Figure 4). In 2D-PMF(φ_1) and (φ_2) profiles we observed that the energy difference between the two minima, corresponding to the right- and left-handed helices, (ΔE_M) is correlated with the $h_{\%}$ and $pop_{h\%}$ values obtained from DSSP and cluster analyses (Table 1) and used here as helix-stabilization indexes. However, the energy barrier between the two minima ($\Delta E_M^{\ddagger}$) is quite high, so their interconversion may be unlikely to occur

at the temperatures and timescale under consideration, provided that this particular reaction coordinate is kinetically relevant.

Conversely, 2D-PMF(ψ_2) and (ψ_3) profiles show a $\Delta E_M^{\ddagger}$ which can be easily overcome. Interestingly, in the 2D-PMF(ψ_3) profiles, both the ΔE_M and $\Delta E_M^{\ddagger}$ values appear to be proportional to $h_{\%}$ and $pop_{h\%}$ (Table 1 and Figure 4). Moreover, a relatively low barrier for the helix/β-strand conformational switch can be observed only for peptides containing, at position 2, Aib, (*R*)-**I** or (1*S*,2*R*,4*R*)-**IV**, suggesting a lower helix-stabilization capability of those CTAAs, compared with the others under discussion.

It should be noted that the peptide model used in the present study, which contains Aib at position 4, was chosen to allow a direct comparison of theoretical results with the previously reported experimental data.[10] However, to assess if the relative helical propensity of CTAAs is influenced by Aib, we also simulated the behavior of an L-Ala pentapeptide substituted at the central position 3 by (*R*)-I or (1*R*,2*R*,4*R*)-**V**, selected as representatives of the least and the most performing CTAAs, respectively.

Table 3. DSSP Helix Content ($h_{\%}$)[a] and H-bond Analyses of 100 ns REMD Trajectories of Ac-L-Ala_2-CTAA-L-Ala_2-NHMe Pentapeptides **16-17**.

			H-Bond		
#	CTAA	$h_{\%}$	donor	acceptor	$occ_{\%}$
16	(*R*)-**I**	42.9±1.4	Ala4	Ala1	32.04
			Ala5	Ala2	35.85
			Ala5	Ala1	7.09
17	(1*R*,2*R*,4*R*)-**V**	81.9±0.4	Ala4	Ala1	38.81
			Ala5	Ala2	60.32
			Ala5	Ala1	5.61

[a] Calculated as the sum of 3_{10}- and α-helix content of CTAA, averaged with respect to the 25-50, 50-75, 75-100 ns time intervals.

As shown by results of DSSP and H-bond analyses reported in Table 3, both CTAAs maintain their ability to stabilize helical secondary structures and, more importantly, their hierarchy in terms of helical propensity is also respected.

Mechanism of helix stabilization. Although PMF analyses provide valuable insights into the folding preferences of peptides containing CTAAs, they do not explain the mechanism of secondary structure stabilization. Compared to natural AAs, all CTAAs are characterized by an additional alkyl group at Cα that is responsible of the limitation of φ_1 conformational freedom, but this does not explain the differences in conformational preference among related CTAAs.[15] The preference of some natural AAs for helical secondary structures have been suggested to be due to side-chain entropic and steric factors,[82-84] as well as the ability to stabilize helical H-bond networks.[55, 85-90] Similar reasons may also contribute to the helix stabilization by CTAAs.

To obtain preliminary information on the structure-"activity" relationships of CTAAs ("activity" implying the ability to induce or stabilize helical conformations), we evaluated the effect of steric hindrance through a 3D quantitative structure-property relationship (QSPR) analysis using the PHASE software.[91-92] This is a well-known medicinal chemistry tool generally used to derive, on the basis of a set of compounds with known activity data, predictive 3D-pharmacophore models.[93]

We aligned ideal models of helix conformations for peptides **1-7**, **9-11, 13-15** (peptides **8** and **12** were excluded since a right-handed helix conformation was not observed by cluster analysis) and performed a 3D-QSPR analysis using $h_{\%}$ from DSSP as the "activity" values (Table S2, S.I.). Results were visualized through a 3D plot showing as blue cubes or red cubes the regions

where hydrophobic substituents positively or negatively affect the helix content, respectively (Figure 5).

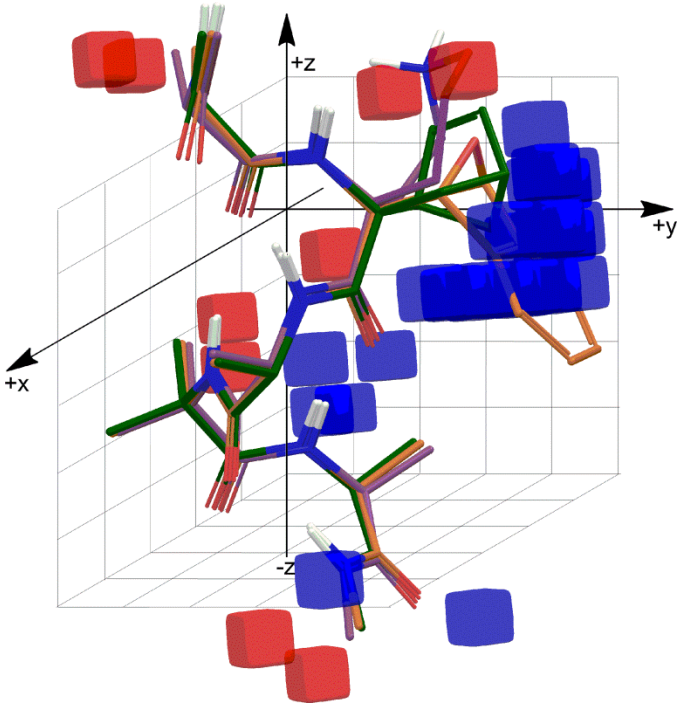

Figure 5. 3D-QSPR regions obtained by PHASE analysis of peptides **1**-**7**, **9**-**11**,**13**-**15**. The blue and red cubes indicate regions where a hydrophobic group increases or decreases, respectively, the helix content. Peptides **1** (purple carbons), **6** (green carbons) and **11** (orange carbons) are shown as a reference.

A positive contribution to the helix stabilization can be exerted by the presence of hydrophobic substituents in the (+x,+y,±z) sector of the right-handed 3D Cartesian space, even though the effect seems to be more evident in the (+x,+y,-z) area, possibly due to the nature of the model peptides under consideration which bear the CTAA at position 2. Steric hindrance that develops along the -z axis should in fact be relevant in limiting the rotational freedom of ψ_2, as evidenced by PMF analyses (Figure 5), and the effect on the downstream dihedrals can be a consequence of this. Indeed, the best performing (1*R*,2*S*,4*R*)-**IIIb** has its aryl group in the (+x,+y,-z) region,

while, its enantiomer, (1*S*,2*R*,4*S*)-**IIIb**, which has a lower helix stabilizing capability, points the aryl group toward the (-x,+y,-z) sector.

In addition, (1*R*,2*R*,4*R*)-**IIIa**, whose aryl group lies in the (-x,+y,+z) region, has $h_{\%}$ and $pop_{h\%}$ lower than (1*R*,2*S*,4*R*)-**IIIb** (Table 1) as well as reduced $\Delta E_M^{\ddagger}$ and ΔE_M in the 2D-PMF profiles (Figure 4), although it is still well performing. Since the plot shown in Figure 5 suggests that steric hindrance in the (-x,+y,+z) region has limited effects, the lower helix-stabilizing ability of (1*R*,2*R*,4*R*)-**IIIa** could be due to its reduced steric hindrance in the (+x,+y,-z) region.

To confirm this hypothesis we evaluated the behavior of a modified CTAA, named (1*R*,2*R*,4*R*)-**IIIawr** (Figure S4, S.I.), where the aromatic ring of the benzoxanorbornene moiety of (1*R*,2*R*,4*R*)-**IIIa** was deleted. As expected, the peptide containing the modified CTAA showed $h_{\%}$ and $pop_{h\%}$ equivalent to those of peptide **3** (Tables 1 and S4, S.I.). The 2D-PMF as a function of φ_1, ψ_2, φ_2 and ψ_3 are comparable, except for a slight difference of 0.5 kcal/mol in ΔE_M in PMF(φ_1) and PMF(ψ_2) (see Figure S5, S.I.).

The same modification was performed to (1*R*,2*S*,4*R*)-**IIIb**, obtaining (1*R*,2*S*,4*R*)-**IIIbwr** (FigureS4, S.I.). As expected, the model peptide maintained a right-handed 3_{10}-helical conformation. However, its $pop_{h\%}$ and $h_{\%}$ were respectively 6 and 4% lower than those of peptide **11** (Tables 1 and S4, S.I.). Moreover, comparing their 2D-PMF(φ_1) and 2D-PMF(ψ) profiles, we observed a slight lowering of ΔE_M and a more significant lowering in the 2D-PMF(φ_1) $\Delta E_M^{\ddagger}$ (Figure S6, S.I.). Actually, the loss in helix-stabilization power of (1*R*,2*S*,4*R*)-**IIIbwr** compared to (1*R*,2*S*,4*R*)-**IIIb** was lower than expected, but this can be explained by observing that the HC=CH bridge of (1*R*,2*S*,4*R*)-**IIIbwr** is still positioned in the (+x,+y,-z) sector and the oxa bridge points towards (+x,+y,+z) (Figure 6A).

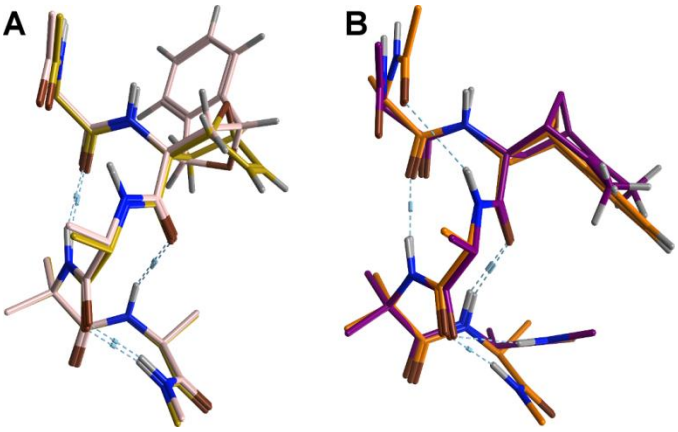

Figure 6. A. Superimposed right-handed 3_{10}-helices of peptides **3** ((1*R*,2*R*,4*R*,)-**IIIa**; pink) and Ala-(1*R*,2*S*,4*R*)-**IIIbwr**-Ala-Aib-Ala (ochre). B. Superimposed right-handed 3_{10}-helices of peptides **11** ((1*R*,2*S*,4*R*)-**IIIb**; orange) and Ala-(1*R*,2*S*,4*R*)-**Vbdm**-Ala-Aib-Ala (purple).

We then evaluated the role of the oxa or methylene bridges by comparing the folding behaviors of model peptides containing (1*R*,2*S*,4*R*)-**Vb** (Figure S5, S.I.), which is the non-isolated regioisomer of (1*R*,2*S*,4*R*)-**V**,[61] and the parent (1*R*,2*S*,4*R*)-**IIIbwr**. We only observed minor differences in cluster and DSSP analyses ($\Delta pop_{h\%} = 1.4$ and $\Delta h_{\%} = 2.6$, both in favor of (1*R*,2*S*,4*R*)-**IIIbwr**; see Tables S3-4, S.I.), as well as in the 2D-PMF(φ) and (ψ) analyses which also showed similar profiles, except for an increased $\Delta E_M^{\ddagger}$ observed in 2D-PMF(φ_1) for (1*R*,2*S*,4*R*)-**Vb** (Figure S7, S.I.), suggesting that this CTAA might disfavor a right-to-left helix conversion.

As a countercheck, we replaced the oxygen bridge in (1*R*,2*S*,4*R*)-**IIIb** by a $-CH_2-$ group, obtaining (1*R*,2*S*,4*R*)-**IIIbmb** (Figure S4). In this case also, we observed significant differences neither in cluster and DSSP analyses of the two model peptides ($\Delta pop_{h\%(IIIb\text{-}IIIbmb)} = -0.5$; $\Delta h_{\%(IIIb\text{-}IIIbmb)} = 1.7$; see Tables 1 and S4, S.I.), nor in 2D-PMF(φ) and (ψ) profiles (Figure S8), so we can conclude that the oxa bridge in the **III** family seems not to play a relevant role in helix-stabilization.

We then investigated whether the positive contribution to helix stabilization of the aryl group in **IIIb** was due to its aromatic nature or merely due to a steric effect. We compared the folding behavior of peptide **11**, containing (1*R*,2*S*,4*R*)-**IIIb**, to that of a model peptide containing the modified CTAA (1*R*,2*S*,4*R*)-**Vbdm** (Figure S4, S.I.), having a methyl group at C5 and C6. Cluster and DSSP analyses showed an improvement of about 7% in the helical content of (1*R*,2*S*,4*R*)-**Vbdm** over (1*R*,2*S*,4*R*)-**Vb** (Tables 1 and S4), with the former getting close to the $pop_{h\%}$ and $h_{\%}$ values of (1*R*,2*S*,4*R*)-**IIIb**. We also observed that the PMF profiles of (1*R*,2*S*,4*R*)-**Vbdm** and (1*R*,2*S*,4*R*)-**IIIb** are closely related, although the former seems to have even more limited conformational freedom (Figure S9, S.I.) that might be ascribed to higher steric hindrance parallel to the z axis (Figure 6B).

(*R*)-**VI** is also a strong helix stabilizer, with $h_{\%}$ and $pop_{h\%}$ about 5% lower than those of (1*R*,2*S*,4*R*)-**IIIb** (Table 1). The superimposed right-handed 3_{10}-helices of peptides **2** and **11** (Figure 7A and C) show that the saturated ring of the tetrahydrocarbazole moiety of (*R*)-**VI** is located in the (+x,+y,-z) area, but the rest of the group lies in the (-x,+y,-z) sector. Indeed, 2D-PMF profiles reproduced those of (1*R*,2*S*,4*R*,)-**IIIb**, but with lower ΔE_M and $\Delta E_M^{\ddagger}$ and increased propensity to the β-strand region, as shown by the PMF(ψ3) profile (Figure 4). The behavior of peptide **4**, having $pop_{h\%}$ and $h_{\%}$ of about 10% lower than **11**, can also be due to the positioning of its benzoxanorbornene core in the (-x,+y,-z) sector (Figure 7).

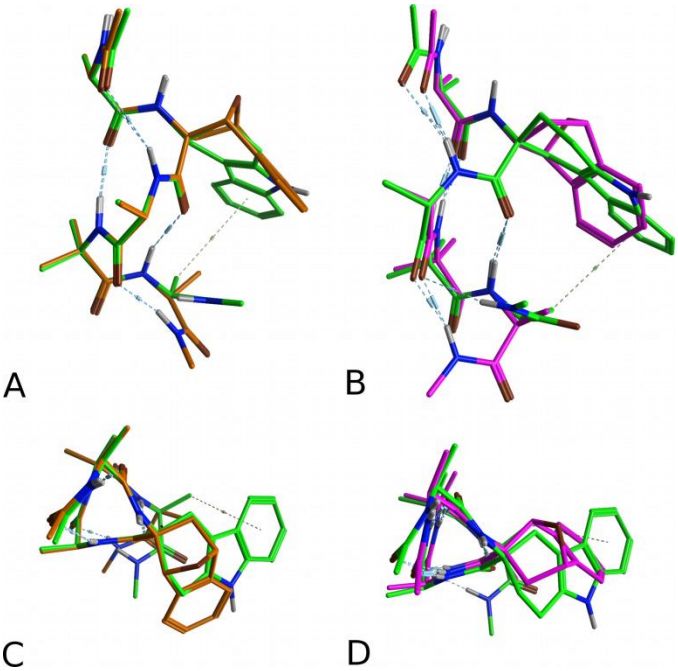

Figure 7. Front (A, B) and top (C, D) views of superimposed right-handed 3_{10}-helices of peptides **7** ((*R*)-**VI**; green), **11** ((1*R*,2*S*,4*R*,)-**IIIb**; orange) and **4** ((1*S*,2*R*,4*S*)-**IIIb**;magenta).

Although steric hindrance is undoubtedly relevant in the helix-stabilization capability of CTAAs, it does not explain the similar behavior of structurally unrelated CTAAs, such as (R)-**VI**, (R)-**II** and (1*R*,2*R*,4*R*)-**V** ($h_{\%}$ =84.1, 85.8 and 82.9%, respectively) as well as the different stabilizing effect predicted for related CTAAs, such as (1*S*,2*R*,4*R*)-**IV** and (1*R*,2*R*,4*R*)-**V** ($h_{\%}$ = 56.5 and 82.9, respectively).

Indeed, the similarly performing (*R*)-**II**, (1*R*,2*R*,4*R*)-**V** and (*R*)-**VI** (Table 1 and Figure S10, S.I.) have their bulky groups in different regions of Cartesian space, with only (*R*)-**VI** partially lying in the (+x,+y,-z) sector. Conversely, the norbornene moiety of (1*R*,2*R*,4*R*)-**V** is located in the (-x,+y,+z) area, which does not seem to affect the helix stabilization, and the indane moiety of (*R*)-**II** lies on the +y axis.

We hypothesized that these results could be due to differences in the intramolecular H-bond networks, as observed for some natural AAs,[55, 57] so we employed QTAIM calculations to find evidence for such differences.

For all the peptides considered here, the BCP network comprised the helical *i+3* → *i* N-H···O BCPs having $\rho(r_c)$ in the typical H-bond range (0.002-0.022 a.u.)[94-95], a positive $\nabla^2(r_c)$, meaning that the interaction is mainly electrostatic, and a low ε, indicating that H-bonds are stable. We observed C_β-H···O *i+3* → *i* BCPs, also occurring in natural peptides,[55, 57] with $\rho(r_c)$ between 0.003-0.009 a.u., which is about one half of the electron density of a typical N-H···O BCP (Tables S6-23, S.I.). Moreover, we observed an additional Aib*4* → Ala3 C_β-H···O BCP (Figure 7) with a $\rho(r_c)$ = 0.011-0.012 a.u., rather a high value for a CH···O interaction involving a hydrogen bound to an sp^3 carbon, which is nonetheless also observable in the extended conformations (Table S9).

Other peculiarities in the QTAIM analyses performed on the right-handed 3_{10}-helices of peptides **2**, **6** and **7** (containing (*R*)-**II**, (1*R*,2*R*,4*R*)-**V** and (*R*)-V**I** at the 2 position, respectively) gave a good explanation of their different behaviors (Tables S6,8,10, S.I.). Indeed, peptide **7** showed only the typical BCP network of helical secondary structures, with a $\sum \rho(r_c)$ = 0.1002 a.u.. Conversely, in peptide **6** we noticed the presence of an additional intra-residue C-H···O BCP, involving the methylene C7-H and the backbone carbonyl group of (1*R*,2*R*,4*R*)-**V**, with a $\rho(r_c)$ = 0.0135 a.u., which is in the range of strong H-bonds (Figure 8 and Table S8).

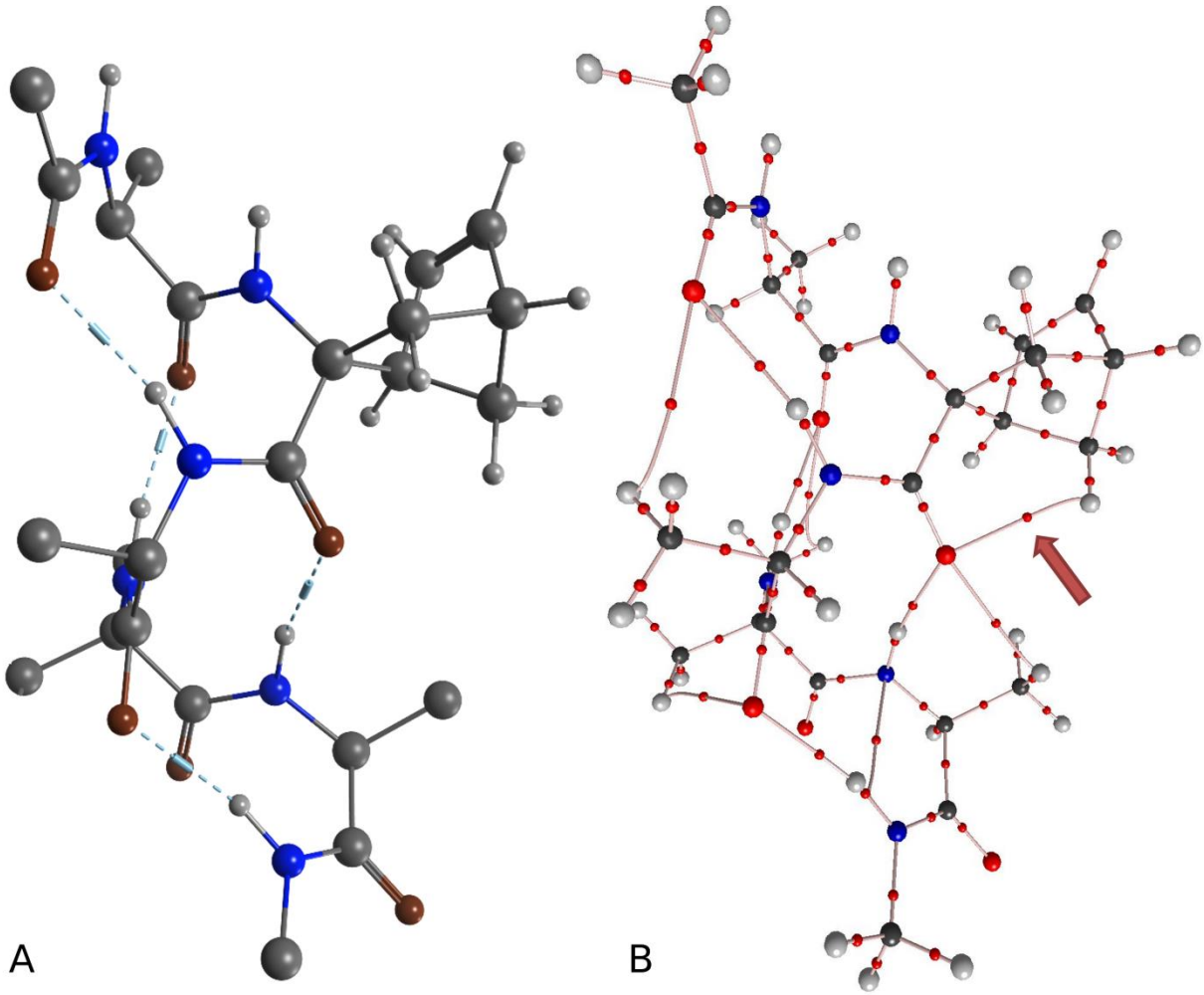

Figure 8. (A) Ball and stick representation and (B) QTAIM molecular graph of the optimized right-handed 3_{10}-helical conformation of Ac-Ala-(1*R*,2*R*,4*R*)-**V**-Ala-Aib-Ala-NHMe. The red arrow indicates the intra-residue C-H···O.

Such an unconventional H-bond is able to constrain the ψ_2 dihedral to a value compatible with a right-handed helix, thus justifying the stability of the helix secondary structure of peptide **6**. Moreover, this intramolecular C-H···O interaction is also evident in the X-ray geometry of an Ac-L-Ala-CTAA-L-Ala-Aib-L-Ala-NH_2 model peptide containing,[59] at the 2-position, a recently synthetized β-benzylsulfanylnorbornene AA (Figure S11, S.I.),[96] providing further validation to our theoretical predictions. Furthermore, a $\Delta\sum\rho\,(r_c)$ = 0.0153 a.u. was found between peptides **6**

and **7**, a difference which is comparable to the $\rho(r_c)$ of a single H-bond, thus suggesting a stronger ability of (1*R*,2*R*,4*R*)-**V** to strengthen the H-bond network. Indeed, it is known that the Gibbs free energy of folding of a protein is of the order of magnitude of a single H-bond.[97]

This hypothesis can also explain the worse performance of (1*R*,2*R*,4*R*)-**IIIa** compared to (1*R*,2*R*,4*R*)-**V** ($\Delta pop_{h\%}$ ~ 10% and $\Delta h\%$ ~3%), although both CTAAs exert steric hindrance in the same sector. Indeed, in peptide **3** we did not observe the intra-residue C-H···O BCP and the $\Delta\sum\rho(r_c)$ between **3** and **6** resulted of 0.0131 a.u. in favor of **6**. Similar results were obtained by comparing peptide **6** with that containing (1*R*,2*R*,4*R*)-**IIIawr** (Tables S8,15, S.I.).

As a further test, we studied the folding behavior of (1*R*,2*R*,4*R*)-**IIIamb**, where the oxygen in position 7 of the (1*R*,2*R*,4*R*)-**IIIa** benzoxanorbornene core was substituted by a methylene group (Figure S4). As expected, the $\sum\rho(r_c)$ of the obtained peptide model resulted equivalent to that of peptide **6** (0.1166 a.u. and 0.1155 a.u., respectively) and an intra-CTAA C-H···O BCP with $\rho(r_c)$ = 0.0137 a.u. was observed (Table S19). This led to an increase in both $pop_{h\%}$ and $helix_{\%}$ of ~10% and 3%, respectively, compared to (1*R*,2*R*,4*R*)-**IIIa** (Tables 1 and S4-5, S.I.). Thus, this modified CTAA proved to be a helix stabilizer as strong as (1*R*,2*R*,4*R*)-**V**.

Regarding peptide **2**, QTAIM analysis showed a $\sum\rho(r_c)$ = 0.1150 a.u. and the presence of a peculiar *i*+*1*→*i* C-H···O BCP with $\rho(r_c)$ = 0.0110 a.u. (Table S6), between C7-H of the aromatic ring of (*R*)-**II** and the carbonyl group of Ala1. Thus, the helix-stabilizing power of (*R*)-**II** is probably due to a combination of its steric hindrance and the additional C-H···O H-bond. However, neither of the two features are fully matched, because the (*R*)-**II** steric hindrance is principally located in the (+x,+y,0) region while the $\rho(r_c)$ of its particular C-H···O BCP is slightly lower than that of the intra-CTAA BCP observed for (1*R*,2*R*,4*R*)-**V**.

Moreover, the PMF(φ_1) and PMF(ψ_2) profiles of peptides **6** and **7** (containing (1*R*,2*R*,4*R*)-**V** and (*R*)-**II**, respectively) are quite different, probably due to the ability of (1*R*,2*R*,4*R*)-**V** to form the intra-CTAA C-H···O interaction, while (*R*)-**II** is involved only in a C-H···O interaction with Ala1, allowing wider conformational freedom to the CTAA backbone.

The comparison of (1*S*,2*R*,4*R*)-**IV** and (1*R*,2*R*,4*R*)-**V** required the study of additional secondary structures. Indeed, despite their apparent structural similarity, peptide **5** showed $\Delta pop_{h\%}$ and $\Delta h_{\%}$ of about 20% lower than **6**. Moreover, we observed that the (1*R*,2*S*,4*S*)-**IV** enantiomer led peptide **12** to a left-handed helix ($pop_{h\%}$ = 30.6%), while a right-handed conformation was obtained for peptide **13**, containing (1*S*,2*S*,4*S*)-**V** (Table 1).

From the 2D-PMF(φ_1) and 2D-PMF(φ_2) profiles of peptides **5** and **6** (Figure S3, S.I.) we noticed that ΔE_M was about 1 and 1.5 kcal/mol lower, respectively, for the former. In addition, both PMF(ψ_2) and (ψ_3) profiles of **5** indicated a reduction in ΔE_M and $\Delta E_M^{\ddagger}$ between the minima corresponding to helical conformations and in $\Delta E^{\ddagger}$ between the helical and extended conformations (Figure 4 and S3). In particular, the ψ_3 dihedral was energetically accessible for the whole ±180 deg. interval.

Consequently, the reasons of the (1*S*,2*R*,4*R*)-**IV** lower helix-stabilization power can be attributed to a reduced stabilization of the right-handed helix and/or to a reduced destabilization of the extended conformation, compared to the related (1*R*,2*R*,4*R*)-**V**

QTAIM analyses on the right-handed 3_{10}-helix of peptides **5** and **6** showed qualitatively similar BCP networks, comprising the *i+3*→*i* N-H···O and *i+3*→*i* C_β-H···O BCPs typical of 3_{10}-helices and the characteristic intra-residue interaction between C7-H and the carbonyl group. However, the BCP network of **6** turned out to be stronger than that of **5**, with a $\Delta\sum\rho(r_c)$ ~

0.0030 a.u., a difference which has been reported as significant to explain the different helix-stabilization propensity of natural AAs (Tables S8-9, S.I.).[55, 97]

Conversely, a $\sum \rho\,(r_c)$ = 0.0073 a.u. was observed between the extended conformations of **5** and **6**, in favor of the former peptide, since the BCP pattern of peptide **6** lacks the C-H···O interaction between C5-H and Ala1, which is instead observable for (1*S*,2*R*,4*R*)-**IV** (Figure S12, S.I.). As a consequence, the extended conformation of peptide **5** is relatively more accessible than that of **6**. Furthermore, it should be emphasized that, although the $\sum \rho\,(r_c)$ for the extended conformations are greater than those for the helical ones, the higher ε values of the BCPs in the extended structures show that the observed interactions are less stable than those in the helices (Tables S8-9, S.I.), confirming a preference for the helix in both cases.

QTAIM analyses also explain the predicted tendency of (1*R*,2*S*,4*S*)-**IV** to stabilize a left-handed helix, while (1*S*,2*S*,4*S*)-**V**, like (1*R*,2*R*,4*R*)-**V**, stabilizes a right-handed helix.[59] Indeed, for peptide **12**, containing (1*R*,2*S*,4*S*)-**IV**, the $\Delta\sum \rho\,(r_c)$ between left- and right-handed helices is 0.0035 a.u., suggesting that the left-handed is favored over the right-handed helix (Tables S8 and S12-15, S.I.). Moreover, although the number of C-H···O interactions is lower for the left-handed helix, these H-bonds are significantly stronger, having values similar to those computed for N-H···O H-bonds. Conversely, a $\Delta\Sigma\rho(r_c)$ of 0.0059 a.u. was found for peptide **13**, containing (1*S*,2*S*,4*S*)-**V**, in favor of the right-handed helix (Table S14-15, S.I.).

Conclusions

There is rising interest in using peptides to produce smart biomaterials as well as innovative drugs, and non-proteinogenic AAs represent a valuable resource for fine-tuning peptide properties. It is thus clear that knowledge of the molecular basis governing the behavior of a

given AA, when inserted into a complex sequence, is desirable to aid the design of new biomolecular tools.

With this study, we aimed to elucidate the mechanism of helix stabilization exerted by a selection of synthetically accessible chiral CTAAs.

Using a combination of REMD simulations and QTAIM analyses, we observed that most of the CTAAs considered were able to stabilize the helical secondary structure of an Ac-L-Ala-CTAA-L-Ala-Aib-L-Ala-NHMe pentapeptide, with a preference for the right-handed 3_{10}-helix. The *R*-Cα enantiomer generally proved a stronger stabilizer of right-handed helices, except for (1*R*,2*S*,4*R*)-**IIIb,** which also turned out to be the strongest helix-stabilizer, though much less accessible synthetically.[48]

We found two complementary mechanisms which can contribute to the reduction of the backbone conformational freedom. The first depends on the steric hindrance exerted by the CTAA in a region somehow parallel to the peptide helix axis, particularly in the area downstream of the CTAA itself, while the second can be ascribed to the strengthening of the helix H-bond network, comprising both classical NH···O=C H-bonds and C-H···O=C interactions.

Chirality at the CTAA Cα was also found to be important. However, the correspondence between stereochemical configuration at Cα and helix-stabilizing power is probably due to the fulfilment of the two mechanisms proposed above. Further investigation of the role of CTAA stereochemistry in determining the preference toward a certain helix screw sense is currently ongoing.

Norbornene CTAA **V** turned out to be interesting for its ability to constrain the φ_1 and ψ_2 dihedrals to values typical of helix geometries through an effective intra-residue C-H···O=C interaction. Moreover, due to its relatively limited steric hindrance, it can be used in peptide synthesis with a reactivity comparable to that of Aib,[59] but allowing the tuning of the peptide molecular shape in order to achieve a better match with the target protein binding surface.

ASSOCIATED CONTENT

AUTHOR INFORMATION

Corresponding Author

* e-mail alessandro.contini@unimi.it

Tel. +39.02.503.14480

Fax. +39.02.503.1447

Author Contributions

The manuscript was written through contributions of all authors. All authors have given approval to the final version of the manuscript.

Notes

The authors declare no competing financial interest.

ACKNOWLEDGMENT

This work was partially supported by Ministero dell'Università e della Ricerca (PRIN 2010 – "Synthesis and biomedical applications of tumor-targeting peptidomimetics." Prot. 2010NRREPL) and by Università degli Studi di Milano (Piano Sviluppo – "Mithocondria

26

targeting peptide based na-nomaterials"). We acknowledge CINECA and Regione Lombardia award, under the LISA initiative, for the availability of high performance computing resources and support.

Supporting Information Available. Supplementary figures and tables; details of cluster, H-bond, DSSP analyses; QTAIM analyses; Cartesian coordinates and energies of QM optimized geometries; Amber force field libraries of CTAAs. This information is available free of charge via the Internet at http://pubs.acs.org.

ABBREVIATIONS

AA, amino acid; CTAA, Cα tetrasubstituted amino acid; REMD, Replica Exchange Molecular Dynamics; QTAIM, Quantum Theory of Atoms In Molecules; DSSP, Define Secondary Structure of Proteins; PMF, Potentials of Mean Force.

REFERENCES

1. Wells, J. A.; McClendon, C. L. Reaching for High-Hanging Fruit in Drug Discovery at Protein-Protein Interfaces. *Nature* **2007,** *450*, 1001-1009.
2. Azzarito, V.; Long, K.; Murphy, N. S.; Wilson, A. J. Inhibition of α-Helix-Mediated Protein-Protein Interactions Using Designed Molecules. *Nature Chem.* **2013,** *5*, 161-173.
3. Pieraccini, S.; Saladino, G.; Cappelletti, G.; Cartelli, D.; Francescato, P.; Speranza, G.; Manitto, P.; Sironi, M. In Silico Design of Tubulin-Targeted Antimitotic Peptides. *Nature Chem.* **2009,** *1*, 642-648.
4. Pellegrino, S.; Ronda, L.; Annoni, C.; Contini, A.; Erba, E.; Gelmi, M. L.; Piano, R.; Paredi, G.; Mozzarelli, A.; Bettati, S. Molecular Insights into Dimerization Inhibition of C-Maf Transcription Factor. *BBA-Proteins Proteom.* **2014,** *1844*, 2108–2115.
5. Venkatraman, J.; Shankaramma, S. C.; Balaram, P. Design of Folded Peptides†. *Chem. Rev.* **2001,** *101*, 3131-3152.
6. Rubinstein, M.; Niv, M. Y. Peptidic Modulators of Protein-Protein Interactions: Progress and Challenges in Computational Design. *Biopolymers* **2009,** *91*, 505-513.
7. Ahrens, V. M.; Bellmann-Sickert, K.; Beck-Sickinger, A. G. Peptides and Peptide Conjugates: Therapeutics on the Upward Path. *Future Med. Chem.* **2012,** *4*, 1567-1586.
8. Diao, L.; Meibohm, B. Pharmacokinetics and Pharmacokinetic-Pharmacodynamic Correlations of Therapeutic Peptides. *Clin. Pharmacokinet.* **2013,** *52*, 855-868.

9. Gentilucci, L.; De Marco, R.; Cerisoli, L. Chemical Modifications Designed to Improve Peptide Stability: Incorporation of Non-Natural Amino Acids, Pseudo-Peptide Bonds, and Cyclization. *Curr. Pharm. Des.* **2010,** *16*, 3185-3203.
10. Pellegrino, S.; Contini, A.; Clerici, F.; Gori, A.; Nava, D.; Gelmi, M. L. 1h-Azepine-4-Amino-4-Carboxylic Acid: A New α,α-Disubstituted Ornithine Analogue Capable of Inducing Helix Conformations in Short Ala-Aib Pentapeptides. *Chem. Eur. J.* **2012,** *18*, 8705-8715.
11. Pellegrino, S.; Contini, A.; Gelmi, M. L.; Lo Presti, L.; Soave, R.; Erba, E. Asymmetric Modular Synthesis of a Semirigid Dipeptide Mimetic by Cascade Cycloaddition/Ring Rearrangement and Borohydride Reduction. *J. Org. Chem.* **2014,** *79*, 3094-3102.
12. Maity, P.; König, B. Enantio- and Diastereoselective Syntheses of Cyclic Cα-Tetrasubstituted α-Amino Acids and Their Use to Induce Stable Conformations in Short Peptides. *Biopolymers (Pept. Sci.)* **2008,** *90*, 8-27.
13. Tanaka, M. Design and Synthesis of Chiral α,α-Disubstituted Amino Acids and Conformational Study of Their Oligopeptides. *Chem. Pharm. Bull.* **2007,** *55*, 349-358.
14. Toniolo, C.; Crisma, M.; Formaggio, F.; Peggion, C. Control of Peptide Conformation by the Thorpe-Ingold Effect (Cα-Tetrasubstitution). *Biopolymers (Pept. Sci.)* **2001,** *60*, 396-419.
15. Toniolo, C.; Formaggio, F.; Kaptein, B.; Broxterman, Q. B. You Are Sitting on a Gold Mine! *Synlett* **2006,** *2006*, 1295-1310.
16. Toniolo, C.; Benedetti, E. The Polypeptide 310-Helix. *Trends Biochem. Sci.* **1991,** *16*, 350-353.
17. Karle, I. L.; Balaram, P. Structural Characteristics of α-Helical Peptide Molecules Containing Aib Residues. *Biochemistry* **1990,** *29*, 6747-6756.
18. Hummel, R.-P.; Toniolo, C.; Jung, G. Conformational Transitions between Enantiomeric 3_{10}-Helices. *Angew. Chem. Int. Ed.* **1987,** *26*, 1150-1152.
19. Kubasik, M.; Blom, A. Acceleration of Short Helical Peptide Conformational Dynamics by Trifluoroethanol in an Organic Solvent. *ChemBioChem* **2005,** *6*, 1187-1190.
20. Kubasik, M.; Kotz, J.; Szabo, C.; Furlong, T.; Stace, J. Helix–Helix Interconversion Rates of Short 13c-Labeled Helical Peptides as Measured by Dynamic Nmr Spectroscopy. *Biopolymers* **2005,** *78*, 87-95.
21. Toniolo, C.; Bonora, G. M.; Barone, V.; Bavoso, A.; Benedetti, E.; Di Blasio, B.; Grimaldi, P.; Lelj, F.; Pavone, V.; Pedone, C. Conformation of Pleionomers of α-Aminoisobutyric Acid. *Macromolecules* **1985,** *18*, 895-902.
22. Longo, E.; Moretto, A.; Formaggio, F.; Toniolo, C. The Critical Main-Chain Length for Helix Formation in Water: Determined in a Peptide Series with Alternating Aib and Ala Residues Exclusively and Detected with Ecd Spectroscopy. *Chirality* **2011,** *23*, 756-760.
23. Karle, I. L. Controls Exerted by the Aib Residue: Helix Formation and Helix Reversal. *Biopolymers (Pept. Sci.)* **2001,** *60*, 351-365.
24. Crisma, M.; Peggion, C.; Moretto, A.; Banerjee, R.; Supakar, S.; Formaggio, F.; Toniolo, C. The 2.05-Helix in Hetero-Oligopeptides Entirely Composed of Cα,α-Disubstituted Glycines with Both Side Chains Longer Than Methyls. *Biopolymers (Pept. Sci.)* **2014,** *102*, 145-158.
25. Boddaert, T.; Sola, J.; Helliwell, M.; Clayden, J. Chemical Communication: Conductors and Insulators of Screw-Sense Preference between Helical Oligo(Aminoisobutyric Acid) Domains. *Chem Commun (Camb)* **2012,** *48*, 3397-3399.
26. Ballano, G.; Zanuy, D.; Jiménez, A. I.; Cativiela, C.; Nussinov, R.; Alemán, C. Structural Analysis of a β-Helical Protein Motif Stabilized by Targeted Replacements with Conformationally Constrained Amino Acids. *J. Phys. Chem. B* **2008,** *112*, 13101-13115.

27. Alemán, C.; Zanuy, D.; Casanovas, J.; Cativiela, C.; Nussinov, R. Backbone Conformational Preferences and Pseudorotational Ring Puckering of 1-Aminocyclopentane-1-Carboxylic Acid. *J. Phys. Chem. B* **2006,** *110*, 21264-21271.
28. Casanovas, J.; Revilla-López, G.; Crisma, M.; Toniolo, C.; Alemán, C. Factors Governing the Conformational Tendencies of Cα-Ethylated α-Amino Acids: Chirality and Side-Chain Size Effects. *J. Phys. Chem. B* **2012,** *116*, 13297-13307.
29. De Poli, M.; De Zotti, M.; Raftery, J.; Aguilar, J. A.; Morris, G. A.; Clayden, J. Left-Handed Helical Preference in an Achiral Peptide Chain Is Induced by an L-Amino Acid in an N-Terminal Type II β-Turn. *J. Org. Chem.* **2013,** *78*, 2248-2255.
30. Demizu, Y.; Doi, M.; Kurihara, M.; Maruyama, T.; Suemune, H.; Tanaka, M. One-Handed Helical Screw Direction of Homopeptide Foldamer Exclusively Induced by Cyclic α-Amino Acid Side-Chain Chiral Centers. *Chem. Eur. J.* **2012,** *18*, 2430-2439.
31. Solà, J.; Morris, G. A.; Clayden, J. Measuring Screw-Sense Preference in a Helical Oligomer by Comparison of 13C NMR Signal Separation at Slow and Fast Exchange. *J. Am. Chem. Soc.* **2011,** *133*, 3712-3715.
32. Pengo, B.; Formaggio, F.; Crisma, M.; Toniolo, C.; Maria Bonora, G.; B. Broxterman, Q.; Kamphuis, J.; Saviano, M.; Iacovino, R.; Rossi, F.*, et al.* Linear Oligopeptides. Part 406.[1] Helical Screw Sense of Peptide Molecules: The Pentapeptide System $(Aib)_4$/L-Val[L-(αMe)Val] in Solution. *J. Chem. Soc., Perkin Trans. 2* **1998**, 1651-1658.
33. Inai, Y.; Kurokawa, Y.; Ida, A.; Hirabayashi, T. Effects of N-Terminal L-Amino Acid Residues on Helical Screw Sense in Achiral Peptides. *Bull. Chem. Soc. Jpn.* **1999,** *72*, 55-61.
34. Inai, Y.; Kurokawa, Y.; Kojima, N. Screw Sense Preference of Non-Polar L-Amino Acid Residues Second from the N-Terminal Position. *J. Chem. Soc., Perkin Trans. 2* **2002**, 1850-1857.
35. Inai, Y.; Ashitaka, S.; Hirabayashi, T. A Study of Chain-Length Effect on Helical Screw Sense in Peptides Having an N-Terminal L-Leu Residue. *Polym J* **1999,** *31*, 246-253.
36. Inai, Y.; Kurokawa, Y.; Hirabayashi, T. Terminal Effect of Chiral Residue on Helical Screw Sense in Achiral Peptides. *Biopolymers* **1999,** *49*, 551-564.
37. Ousaka, N.; Takeyama, Y.; Iida, H.; Yashima, E. Chiral Information Harvesting in Dendritic Metallopeptides. *Nature Chem.* **2011,** *3*, 856-861.
38. De Poli, M.; Byrne, L.; Brown, R. A.; Solà, J.; Castellanos, A.; Boddaert, T.; Wechsel, R.; Beadle, J. D.; Clayden, J. Engineering the Structure of an N-Terminal β-Turn to Maximize Screw-Sense Preference in Achiral Helical Peptide Chains. *J. Org. Chem.* **2014,** *79*, 4659-4675.
39. Le Bailly, B. A. F.; Clayden, J. Controlling the Sign and Magnitude of Screw-Sense Preference from the C-Terminus of an Achiral Helical Foldamer. *Chem. Commun.* **2014,** *50*, 7949-7952.
40. Brown, R. A.; Marcelli, T.; De Poli, M.; Solà, J.; Clayden, J. Induction of Unexpected Left-Handed Helicity by an N-Terminal L-Amino Acid in an Otherwise Achiral Peptide Chain. *Angew. Chem. Int. Ed.* **2012,** *51*, 1395-1399.
41. Byrne, L.; Solà, J.; Boddaert, T.; Marcelli, T.; Adams, R. W.; Morris, G. A.; Clayden, J. Foldamer-Mediated Remote Stereocontrol: >1,60 Asymmetric Induction. *Angew. Chem. Int. Ed.* **2014,** *53*, 151-155.
42. Clayden, J.; Castellanos, A.; Solà, J.; Morris, G. A. Quantifying End-to-End Conformational Communication of Chirality through an Achiral Peptide Chain. *Angew. Chem. Int. Ed.* **2009,** *48*, 5962-5965.

43. Demizu, Y.; Doi, M.; Kurihara, M.; Okuda, H.; Nagano, M.; Suemune, H.; Tanaka, M. Conformational Studies on Peptides Containing A,A-Disubstituted A-Amino Acids: Chiral Cyclic A,A-Disubstituted A-Amino Acid as an A-Helical Inducer. *Org. Biomol. Chem.* **2011,** *9*, 3303-3312.
44. Ruffoni, A.; Casoni, A.; Pellegrino, S.; Gelmi, M. L.; Soave, R.; Clerici, F. Sulfanyl-Methylene-5(4H)-Oxazolones and β-Sulfanyl-α-Nitroacrylates as Appealing Dienophiles for the Synthesis of Conformationally Constrained Cysteine Analogues. *Tetrahedron* **2012,** *68*, 1951-1962.
45. Pellegrino, S.; Clerici, F.; Gelmi, M. L. β-Hydroxynorbornane Amino Acid Derivatives: Valuable Synthons for the Diastereoselective Preparation of Substituted Cyclopentylglycine Derivatives. *Tetrahedron* **2008,** *64*, 5657-5665.
46. Gelmi, M. L.; Cattaneo, C.; Pellegrino, S.; Clerici, F.; Montali, M.; Martini, C. An Efficient Route to All Stereoisomeric Enantiopure 6-Amino-3-Alkyl-3-Azabicyclo[3.2.1]Octane-6-Carboxylic Acids. *J. Org. Chem.* **2007,** *72*, 9811-9814.
47. Ma, D.; Ding, K.; Tian, H.; Wang, B.; Cheng, D. Asymmetric Synthesis of (*S*)-1-Aminoindan-1,5-Dicarboxylic Acid and Related Analogues Via Intramolecular Acylation of Enantiopure α,α-Disubstituted Amino Acids. *Tetrahedron: Asymmetry* **2002,** *13*, 961-969.
48. Yamazaki, H.; Horikawa, H.; Nishitani, T.; Iwasaki, T.; Nosaka, K.; Tamaki, H. Syntheses and Antiulcer Activities of 2-Aminonorbornene Derivatives. *Chem. Pharm. Bull.* **1992,** *40*, 102-108.
49. Sugita, Y.; Okamoto, Y. Replica-Exchange Molecular Dynamics Method for Protein Folding. *Chem. Phys. Lett.* **1999,** *314*, 141-151.
50. Shell, M. S.; Ritterson, R.; Dill, K. A. A Test on Peptide Stability of Amber Force Fields with Implicit Solvation. *J. Phys. Chem. B* **2008,** *112*, 6878-6886.
51. Ding, F.; Tsao, D.; Nie, H.; Dokholyan, N. V. Ab Initio Folding of Proteins with All-Atom Discrete Molecular Dynamics. *Structure* **2008,** *16*, 1010-1018.
52. Lin, E.; Shell, M. S. Convergence and Heterogeneity in Peptide Folding with Replica Exchange Molecular Dynamics. *J. Chem. Theory Comput.* **2009,** *5*, 2062-2073.
53. Bader, R. F. W., *Atoms in Molecules: A Quantum Theory*. Clarendon: Oxford, UK, 1990.
54. Plevin, M. J.; Bryce, D. L.; Boisbouvier, J. Direct Detection of CH/Π Interactions in Proteins. *Nature Chem.* **2010,** *2*, 466-471.
55. LaPointe, S. M.; Farrag, S.; Bohórquez, H. J.; Boyd, R. J. QTAIM Study of an α-Helix Hydrogen Bond Network. *J. Phys. Chem. B* **2009,** *113*, 10957-10964.
56. Parthasarathi, R.; Raman, S. S.; Subramanian, V.; Ramasami, T. Bader's Electron Density Analysis of Hydrogen Bonding in Secondary Structural Elements of Protein. *J. Phys. Chem. A* **2007,** *111*, 7141-7148.
57. Vener, M. V.; Egorova, A. N.; Fomin, D. P.; Tsirelson, V. G. QTAIM Study of the Closed-Shell Interactions in Peptide Secondary Structures: A Cluster Treatment of Oligo- and Polyalanines. *Chem. Phys. Lett.* **2007,** *440*, 279-285.
58. Jiménez, A. I.; Cativiela, C.; Gómez-Catalán, J.; Pérez, J. J.; Aubry, A.; París, M.; Marraud, M. Influence of Side Chain Restriction and NH···Π Interaction on the β-Turn Folding Modes of Dipeptides Incorporating Phenylalanine Cyclohexane Derivatives. *J. Am. Chem. Soc.* **2000,** *122*, 5811-5821.
59. Ruffoni, A.; Contini, A.; Maffucci, I.; Soave, R.; Esposto, I.; Pellegrino, S.; Gelmi, M. L.; Clerici, F. Synthesis and Conformational Analysis of Model Peptides Containing the 3-

Sulfanyl-Norbornen Amino Acid, an Effective Inducer of 3_{10}-Helix Secondary Structures. *submitted* **2014**.
60. Cativiela, C.; López, P.; Mayoral, J. Asymmetric Synthesis of Cycloaliphatic α-Amino Acids with a Norbornane Skeleton. *Tetrahedron: Asymmetry* **1990,** *1*, 379-388.
61. Caputo, F.; Clerici, F.; Gelmi, M. L.; Pellegrino, S.; Pocar, D. An Efficient Synthesis of New Diastereomeric Enantiopure 1-Aminocyclopentane-1,2,4-Tricarboxylic Acids. *Tetrahedron: Asymmetry* **2006,** *17*, 1430-1436.
62. Maki, Y.; Masugi, T.; Hiramitsu, T.; Ogiso, T. Studies of Alicyclic α-Amino Acids. III. Synthesis and Biological Evaluation of 3-Amino-1,2,3,4-Tetrahydrocarbazole-3-Carboxylic Acids. *Chem. Pharm. Bull.* **1973,** *21*, 2460-2465.
63. *Molecular Operating Environment (MOE)*, 2013.08; Chemical Computing Group Inc.: 1010 Sherbooke St. West, Suite #910, Montreal, QC, Canada, H3A 2R7, 2013.
64. Dupradeau, F.-Y.; Pigache, A.; Zaffran, T.; Savineau, C.; Lelong, R.; Grivel, N.; Lelong, D.; Rosanski, W.; Cieplak, P. The R.E.D. Tools: Advances in RESP and ESP Charge Derivation and Force Field Library Building. *Phys. Chem. Chem. Phys.* **2010,** *12*, 7821-7839.
65. Hornak, V.; Abel, R.; Okur, A.; Strockbine, B.; Roitberg, A.; Simmerling, C. Comparison of Multiple Amber Force Fields and Development of Improved Protein Backbone Parameters. *Proteins: Struct., Funct., Bioinf.* **2006,** *65*, 712-725.
66. Francis, A. K.; Iqbal, M.; Balaram, P.; Vijayan, M. Crystal Structure of Boc-Ala-Aib-Ala-Aib-Aib-Methyl Ester, a Pentapeptide Fragment of the Channel-Forming Ionophore Suzukacillin. *Biopolymers* **1983,** *22*, 1499-1505.
67. Beauchamp, K. A.; Lin, Y.-S.; Das, R.; Pande, V. S. Are Protein Force Fields Getting Better? A Systematic Benchmark on 524 Diverse NMR Measurements. *J. Chem. Theory Comput.* **2012,** *8*, 1409-1414.
68. Cino, E. A.; Choy, W.-Y.; Karttunen, M. Comparison of Secondary Structure Formation Using 10 Different Force Fields in Microsecond Molecular Dynamics Simulations. *J. Chem. Theory Comput.* **2012,** *8*, 2725-2740.
69. Lange, O. F.; van der Spoel, D.; de Groot, B. L. Scrutinizing Molecular Mechanics Force Fields on the Submicrosecond Timescale with NMR Data. *Biophys. J.* **2010,** *99*, 647-655.
70. Best, R. B.; Buchete, N.-V.; Hummer, G. Are Current Molecular Dynamics Force Fields Too Helical? *Biophys. J.* **2008,** *95*, L07-L09.
71. Onufriev, A.; Bashford, D.; Case, D. A. Exploring Protein Native States and Large-Scale Conformational Changes with a Modified Generalized Born Model. *Proteins Struct. Funct. Bioinf.* **2004,** *55*, 383-394.
72. Case, D. A.; Darden, T. A.; Cheatham, T. E., III; Simmerling, C.; Wang, J.; Duke, R. E.; Luo, R.; Walker, R. C.; Zhang, W.; Merz, K. M.*, et al. AMBER 12*, University of California, San Francisco, 2012.
73. Caliński, T.; Harabasz, J. A Dendrite Method for Cluster Analysis. *Commun. Stat.* **1974,** *3*, 1-27.
74. Kabsch, W.; Sander, C. Dictionary of Protein Secondary Structure: Pattern Recognition of Hydrogen-Bonded and Geometrical Features. *Biopolymers* **1983,** *22*, 2577-2637.
75. Humphrey, W.; Dalke, A.; Schulten, K. Vmd: Visual Molecular Dynamics. *J. Mol. Graphics Modell.* **1996,** *14*, 33-38.
76. Grossfield, A. *WHAM: The Weighted Histogram Analysis Method*, version 2.0.9.

77. Frisch, M. J.; Trucks, G. W.; Schlegel, H. B.; Scuseria, G. E.; Robb, M. A.; Cheeseman, J. R.; Scalmani, G.; Barone, V.; Mennucci, B.; Petersson, G. A*., et al. Gaussian 09, Revision A.1*, Gaussian, Inc.: Wallingford CT, 2009.
78. Zhao, Y.; Truhlar, D. G. Hybrid Meta Density Functional Theory Methods for Thermochemistry, Thermochemical Kinetics, and Noncovalent Interactions: The MPW1B95 and MPWB1K Models and Comparative Assessments for Hydrogen Bonding and van Der Waals Interactions. *J. Phys. Chem. A* **2004,** *108*, 6908-6918.
79. Contini, A.; Erba, E. Click-Chemistry Approach to Azacycloalkene Monosulfonyl Diamines: Synthesis and Computational Analysis of the Reaction Mechanism. *RSC Advances* **2012,** *2*, 10652-10660.
80. Cossi, M.; Rega, N.; Scalmani, G.; Barone, V. Energies, Structures, and Electronic Properties of Molecules in Solution with the C-PCM Solvation Model. *J. Comput. Chem.* **2003,** *24*, 669-681.
81. Biegler-König, F.; Schönbohm, J.; Bayles, D. AIM2000. *J. Comput. Chem.* **2001,** *22*, 545-559.
82. Avbelj, F.; Moult, J. Role of Electrostatic Screening in Determining Protein Main Chain Conformational Preferences. *Biochemistry* **1995,** *34*, 755-764.
83. Hermans, J.; Anderson, A. G.; Yun, R. H. Differential Helix Propensity of Small Apolar Side Chains Studied by Molecular Dynamics Simulations. *Biochemistry* **1992,** *31*, 5646-5653.
84. Wang, J.; Purisima, E. O. Analysis of Thermodynamic Determinants in Helix Propensities of Nonpolar Amino Acids through a Novel Free Energy Calculation. *J. Am. Chem. Soc.* **1996,** *118*, 995-1001.
85. Shi, Z.; Olson, C. A.; Bell, A. J.; Kallenbach, N. R. Stabilization of α-Helix Structure by Polar Side-Chain Interactions: Complex Salt Bridges, Cation–Π Interactions, and C–H … O H-Bonds. *Biopolymers (Pept. Sci.)* **2001,** *60*, 366-380.
86. Chang, C.; Bader, R. F. W. Theoretical Construction of a Polypeptide. *J. Phys. Chem.* **1992,** *96*, 1654-1662.
87. Scheiner, S. Contributions of NH···O and CH···O Hydrogen Bonds to the Stability of β-Sheets in Proteins. *J. Phys. Chem. B* **2006,** *110*, 18670-18679.
88. Scheiner, S.; Kar, T.; Pattanayak, J. Comparison of Various Types of Hydrogen Bonds Involving Aromatic Amino Acids. *J. Am. Chem. Soc.* **2002,** *124*, 13257-13264.
89. Manikandan, K.; Ramakumar, S. The Occurrence of C-H…O Hydrogen Bonds in α-Helices and Helix Termini in Globular Proteins. *Proteins Struct. Funct. Bioinf.* **2004,** *56*, 768-781.
90. Wahl, M. C.; Sundaralingam, M. C-H…O Hydrogen Bonding in Biology. *Trends Biochem. Sci.* **1997,** *22*, 97-102.
91. Dixon, S.; Smondyrev, A.; Knoll, E.; Rao, S.; Shaw, D.; Friesner, R. PHASE: A New Engine for Pharmacophore Perception, 3D QSAR Model Development, and 3D Database Screening: 1. Methodology and Preliminary Results. *J. Comput. Aided. Mol. Des.* **2006,** *20*, 647-671.
92. Dixon, S. L.; Smondyrev, A. M.; Rao, S. N. PHASE: A Novel Approach to Pharmacophore Modeling and 3D Database Searching. *Chem. Biol. Drug. Des.* **2006,** *67*, 370-372.
93. Leone, S.; Mutti, C.; Kazantsev, A.; Sturlese, M.; Moro, S.; Cattaneo, E.; Rigamonti, D.; Contini, A. SAR and QSAR Study on 2-Aminothiazole Derivatives, Modulators of Transcriptional Repression in Huntington's Disease. *Bioorg. Med. Chem.* **2008,** *16*, 5695-5703.

94. Koch, U.; Popelier, P. L. A. Characterization of C-H-O Hydrogen Bonds on the Basis of the Charge Density. *J. Phys. Chem.* **1995,** *99*, 9747-9754.
95. Tang, T. H.; Hu, W. J.; Yan, D. Y.; Cui, Y. P. A Quantum Chemical Study on Selected Π-Type Hydrogen-Bonded Systems. *J. Mol. Struct.* **1990,** *207*, 319-326.
96. Ruffoni, A.; Ferri, N.; Bernini, S. K.; Ricci, C.; Corsini, A.; Maffucci, I.; Clerici, F.; Contini, A. 2-Amino-3-(Phenylsulfanyl)Norbornane-2-Carboxylate: An Appealing Scaffold for the Design of Rac1-Tiam1 Protein-Protein Interaction Inhibitors. *J. Med. Chem.* **2014,** *57*, 2953-2962.
97. Wang, Z.-X.; Wu, C.; Lei, H.; Duan, Y. Accurate Ab Initio Study on the Hydrogen-Bond Pairs in Protein Secondary Structures. *J. Chem. Theory Comput.* **2007,** *3*, 1527-1537.

SYNOPSYS